Int. J. Heat Mass Transfer. Vol. 33, No. 5, pp. 1013–1023, 1990
Printed in Great Britain

0017-9310/90 $3.00 + 0.00

Effect of wall conduction on free convection between asymmetrically heated vertical plates: uniform wall heat flux

S. H. KIM and N. K. ANAND
Department of Mechanical Engineering, Texas A&M University, College Station, TX 77843, U.S.A.

and

WIN AUNG
Division of Mechanical and Structural Systems, National Science Foundation, Washington, DC 20550, U.S.A.

(*Received* 13 *January* 1989 *and in final form* 5 *September* 1989)

Abstract—In this study of the effect of wall conduction on laminar free convection between asymmetrically heated vertical plates, an implicit finite difference scheme is used to solve the governing equations. The governing independent parameters are identified to be Prandtl number (Pr), Grashof number (Gr), ratio of thermal conductivity of the solid to air (K), wall thickness to channel width ratio (t/B), channel height to width ratio (L/B) and the asymmetric heating parameter (γ_H). The effect of wall conduction on free convective flow of air under asymmetrically heated conditions ($\gamma_H = 1.0$, 0.5, and 0) is discussed. Calculations are made for $K = 1$ and 10, $t/B = 0.1$ and 0.5, $Gr = 10$–10^4, and $L/B = 1$ and 5. The maximum increase in mass flow rate of air for symmetric heating due to wall conduction is 30%. The maximum decrease in average Nusselt number due to wall conduction is 22%. Wall conduction effects are more significant for low Gr flows than for high Gr flows.

INTRODUCTION

CONSIDERABLE attention has been given to laminar free convection in vertical channels. In the recent past there has been a renewed interest in this topic because of its applications to cooling of electronic circuit boards used in modern computers. Depending on the nature of the approach to this problem, the literature can be classified into experimental and numerical work. Experimental studies of laminar free convection between parallel heated vertical plates [1–4] consider both symmetric and asymmetric heating conditions. Finite difference methods were used to study laminar free convection by some investigators [5–7]. These calculations were made by solving boundary layer equations between vertical plates. Some other investigators conducted both experiments and computations to study free convection between parallel plates [8–11].

A careful examination of the literature reveals that Burch *et al.* [12] were the only ones to study the impact of wall conduction on laminar free convection between parallel plates. A control volume based finite difference method was used to solve the governing equations. Consideration was given only to symmetric heating conditions and external surfaces of the plates were subjected to uniform wall temperature conditions (UWT). A range of geometrical, wall conduction, and heat transfer parameters were addressed. Calculations were made for the Grashof number (Gr) range of 10–10^6. This study showed that wall conduction has a significant impact on the heat transfer at high Grashof numbers, low conductivity ratios, and high wall thickness to channel width ratios.

The objective of the present work is to numerically study the effect of wall conduction on laminar free convection between parallel vertical plates subjected to asymmetric heating. Plates are heated by subjecting the external surfaces of the plates to uniform heat flux (UHF) conditions. An implicit finite difference scheme has been developed to solve the governing equations. In the following sections the model development, solution methodology, validation of the solution methodology and results of parametric studies are discussed.

MODEL DEVELOPMENT

The geometrical configuration for analysis is shown in Fig. 1. Only steady-state, laminar free convection is considered. The external surfaces of the left and right walls are heated to UHF conditions in channels with unequal (asymmetric) wall heating. The temperature difference between the walls and the air at the channel inlet is the driving force for air flow. Thermo-physical properties of air are assumed to remain constant, except for the density. The Boussinesq approximation is invoked, thereby confining the density variation to the buoyancy term in the axial

NOMENCLATURE

B	channel width
Gr	Grashof number
k	thermal conductivity
K	ratio of thermal conductivity of solid wall to the thermal conductivity of air
L	channel height
M	mass flow rate of air
Nu	Nusselt number
P	non-dimensional pressure
p	dimensional pressure of air
Pr	Prandtl number
q	non-dimensional heat flux
q'	dimensional heat flux
t	wall thickness
T	dimensional temperature
u	dimensional velocity in the axial direction
v	dimensional velocity in the transverse direction
U, V	non-dimensional velocities
x	axial coordinate
y	transverse coordinate
X, Y	non-dimensional coordinates.

Greek symbols

β	thermal expansion coefficient
γ_H	asymmetric heating parameter
θ	non-dimensional temperature
μ	viscosity
ν	kinematic viscosity
ρ	density.

Subscripts

a	air
e	external surface
exit	channel exit
i	interface
l	left wall (hot side)
max	maximum value
min	minimum value
r	right wall (cold side)
s	solid
0	channel inlet.

Superscript

$\bar{}$	average value.

momentum equation. The temperature fields of air and the solid walls are coupled because temperature and heat flux are continuous at both the left and right interfaces. The temperature field of air is coupled to its axial momentum equation by the buoyancy term, and the continuity equation for air is linked to the axial momentum equation by the velocity field. The pressure variation in the transverse direction is assumed to be negligible. Based on these simplifying assumptions and discussion, the model equations in non-dimensional terms can be written as:

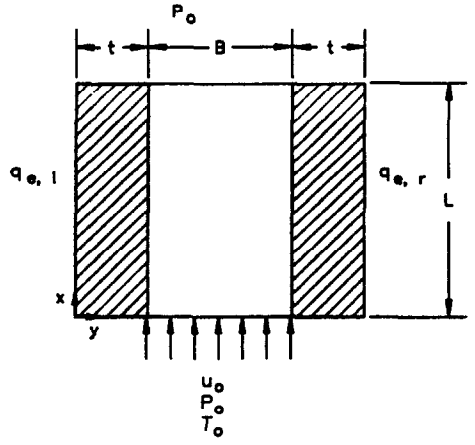

FIG. 1. Physical model.

continuity—air

$$\frac{\partial U}{\partial X}+\frac{\partial V}{\partial Y}=0; \tag{1}$$

axial momentum—air

$$U\frac{\partial U}{\partial X}+V\frac{\partial U}{\partial Y}=-\frac{\partial P}{\partial X}+\frac{\partial^2 U}{\partial Y^2}+\theta; \tag{2}$$

energy—air

$$U\frac{\partial \theta}{\partial X}+V\frac{\partial \theta}{\partial Y}=\frac{1}{Pr}\frac{\partial^2 \theta}{\partial Y^2}; \tag{3}$$

energy—solid

$$K\left[\frac{\partial^2 \theta}{\partial X^2}+\frac{L^2 Gr^2}{B^2}\frac{\partial^2 \theta}{\partial Y^2}\right]=0 \tag{4}$$

where

$$X=\frac{x}{L\,Gr},\quad Y=\frac{y}{B}$$

$$U=\frac{B^2 u}{Lv\,Gr},\quad V=\frac{Bv}{v}$$

$$P=\frac{(p-p_0)B^4}{\rho L^2 v^2\,Gr},\quad Pr=\frac{\mu_a C_{p,a}}{k_a}$$

$$\theta=\frac{(T-T_0)}{q_{e,l}B/k_a},\quad Gr=\frac{g\beta q_{e,l}B^5}{Lv^2 k_a}. \tag{4a}$$

The model equations form a set of four coupled partial differential equations. The U-velocity field is elliptic in the transverse direction and is assumed to have a parabolic behavior in the stream-wise (X)

direction, warranting specification of the U-velocities at the channel inlet and the interfaces. The U-velocities are zero at both the left and right interfaces because of the no-slip conditions. The U-velocity at the channel inlet is unknown. Only the first derivative of pressure appears in the axial momentum equation, requiring P to be specified only at the entrance. Non-dimensional pressure is known to be zero ($P = 0$) at the exit ($X = 1/Gr$) of the channel and is assumed to be zero at the channel inlet; it is unknown and must be part of the solution. The extra information available on pressure ($P = 0$, $X = 1/Gr$) alleviates the difficulty of not knowing U at $X = 0$.

In the solution process, a uniform velocity U_0 at the channel inlet is estimated and computations are made by marching in the X-direction. The calculated non-dimensional pressure at the channel exit should be zero; if not, the estimated value U_0 is changed and calculations are repeated until P is zero at the channel exit. The V-velocity is zero at the left and right interfaces because of the no-slip condition and also at the channel inlet since uniform velocity U_0 is assumed to prevail across the channel width. Note that at $X = 0$, p is not equal to p_0 and can be determined from the potential flow theory to be equal to $-\rho u_0^2/2$. Sample calculations with $p = -\rho u_0^2/2$ at $X = 0$ indicated that the results did not vary significantly for the range of $Gr(\leqslant 10^4)$ and $L/B(\leqslant 5)$.

The energy equation for air is elliptic in the transverse (Y) direction and assumed parabolic in the axial direction. Since heat flux and temperature are continuous at both the left and right interfaces

$$K\frac{\partial\theta}{\partial Y} = -\frac{\partial\theta}{\partial Y}\text{(left interface)}$$

$$K\frac{\partial\theta}{\partial Y} = +\frac{\partial\theta}{\partial Y}\text{(right interface).} \qquad (5)$$

The non-dimensional temperature θ at the channel inlet is zero ($\theta = 0$, $X = 0$). A single energy equation describes the temperature distribution in the left and right walls (equation (4)). This equation is elliptic in both the axial and transverse directions. The top and bottom surfaces of both walls are treated as adiabatic. Boundary conditions at the external surface of the plates are

$$K\frac{\partial\theta}{\partial Y} = -1 \text{ (external surface of the left wall)} \qquad (6)$$

$$K\frac{\partial\theta}{\partial Y} = \gamma_H \text{ (external surface of the right wall).} \qquad (7)$$

In equation (7), γ_H represents the asymmetric heating parameter ($\gamma_H = q_{c,r}/q_{c,l}$).

SOLUTION TECHNIQUE

The dependent variables are U, V, P, and θ; the independent variables are essentially spatial coordinates. Hence, there are four unknowns and four partial differential equations, equations (1)–(4). The axial momentum equation is coupled with the air temperature field by the buoyancy term. The air temperature field is coupled to the solid temperature field by the interface heat flux and temperature continuity requirement. Since the coupled and non-linear nature of these equations precludes the use of a closed form solution technique, this set of equations is solved by a fully implicit finite difference technique.

The solution procedure has two steps: (1) discretization of the partial differential equations into linear algebraic equations, and (2) solution of a set of simultaneous equations to obtain the pressure, velocity, and temperature fields. The governing equations for air (equations (1)–(3)) display elliptic behavior in the Y-direction and parabolic behavior in the X-direction. The energy equation for the solid displays elliptic behavior in both the X- and Y-directions. In the axial momentum equation for air, the derivatives in the X-direction are replaced by first-order, forward difference expressions; derivatives in the Y-direction are replaced by second-order, central difference expressions. The same procedure is adopted to obtain the finite difference form of the energy equation for air (equation (3)). The derivatives in the energy equation for the solid (includes both left and right plates) are replaced by the second-order, central difference expressions.

Examination of the governing equations for air reveals three governing equations (continuity, momentum, and energy) and four unknowns (U, V, P, and θ). The parabolic behavior of these equations enables marching the computations in the axial direction. The mass flow rate of air at each stream-wise location is constant because of steady-state conditions. Hence, the integral form of the continuity equation

$$\int_{Y_{i,l}}^{Y_{i,r}} U\,dY = U_0 \qquad (8)$$

makes up for the missing equation. The algebraic form of equation (8) is obtained by replacing it with Simpson's one-third rule. The computational sequence is as follows.

(1) The inlet velocity U_0 is estimated and treated as uniform across the channel.

(2) The axial momentum equation (equation (2)) and the integral form of the continuity equation (equation (8)) for air at each marching station between the channel inlet and exit are solved to obtain U and P. The coupled algebraic equations at each marching station are transformed to an upper triangle matrix form and consequently solved by the Gauss elimination technique.

(3) With the differential form of the continuity equation for air (equation (1)), the values of V-velocity are obtained everywhere.

(4) The energy equation for air (equation (3)) and solid (equation (4)) and with the interface conditions

(equation (5)) are solved to obtain the air and solid temperatures. Note that although solid and air temperatures are coupled, one is elliptic (equation (4)), and the other is parabolic (equation (3)). The finite difference forms of these equations are solved by sweeping in the cross-stream (Y) and axial (X) directions. In each of these sweeps, the resulting equations are solved by the tri-diagonal matrix algorithm. In sweeping in the cross-stream direction, the air temperature field is not considered. In sweeping in the axial direction, the temperature fields of both air and solid are included.

(5) Steps 2–4 are repeated until the maximum difference of temperatures between two successive iterative steps at any location is less than 10^{-6}.

(6) If $P_{ext}/|P_{min}| < 5 \times 10^{-5}$, convergence is declared. If not, the estimated value of the inlet velocity, U_0, is altered and steps 2–6 are repeated. P_{min} is the minimum value of P in the domain.

VALIDATION OF THE SOLUTION TECHNIQUE

A number of numerical experiments were conducted to establish the grid independent solution. In the transverse direction, 91 uniform grid points were deployed. Forty grid points were placed in the solid and 51 in the air domain. In the axial direction, the step size at the channel entrance was made equal to 0.1% of the total length ($L = 1/Gr$) of the channel, and the step size was expanded gradually with an expansion factor of 3%. For this grid size the sum of the average of the left and right local interface heat flux values was within 3% of the sum of the heat flux values imposed on the external surfaces of the left and right walls.

The solution scheme is validated by comparing the average mass flow rate and the average Nusselt number for the case of no wall conduction with the calculations of ref. [10]. As shown in Figs. 2(a) and (b), the difference between the two calculations is negligible. The average mass flow rate is defined by

$$\bar{M} = \frac{2}{(1+\gamma_H)} \int_{Y_{i,l}}^{Y_{i,r}} U \, dY. \tag{9}$$

The average Nusselt number for the channel is given by

$$\overline{Nu} = \frac{(q_{e,l}+q_{e,r})/2}{(\bar{\theta}_{i,l}+\bar{\theta}_{i,r})/2} \tag{10}$$

where

$$\bar{\theta}_{i,l} = \int_0^{1/Gr} \theta_{i,l} \, dX \tag{11}$$

and

$$\bar{\theta}_{i,r} = \int_0^{1/Gr} \theta_{i,r} \, dX. \tag{12}$$

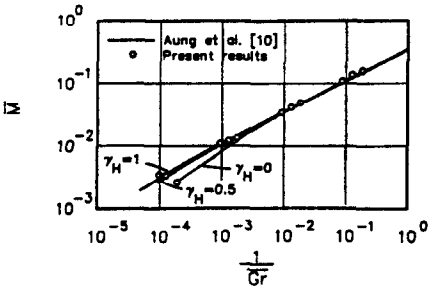

FIG. 2(a). Mass flow rate.

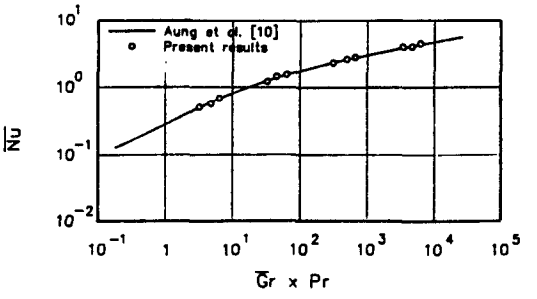

FIG. 2(b). Average Nusselt number.

RESULTS AND DISCUSSION

Independent parameters

Examination of the governing equations reveals that the independent parameters are Grashof number (Gr), Prandtl number (Pr), wall thickness to channel width (t/B), channel length to channel width ratio (L/B), ratio of the thermal conductivity of the wall to the thermal conductivity of the fluid (K), and the asymmetric heating parameter (γ_H). The independent variables are the spatial coordinates. In considering only flow of air in the channel, Pr was fixed at 0.7. The Grashof number (Gr) was varied between 10 and 10^4. Because the higher values of Gr ($> 10^4$) required extremely small step sizes in the channel entrance, and hence a prohibitively large CPU time for the computations, calculations were confined to $Gr \leqslant 10^4$. The effect of wall conduction on heat transfer and the flow field is studied by calculating for $K = 1$ and 10, $t/B = 0.1$ and 0.5, and $L/B = 1$ and 5. Calculations were made for asymmetric heating parameter (γ_H) values of 0, 0.5, and 1. $\gamma_H = 1$ corresponds to a symmetric heating case, and $\gamma_H = 0$ implies that the external surface of the right wall is subjected to an adiabatic condition. For $\gamma_H < 1$, the left and right walls are referred to as hot and cold walls, respectively.

The effects of wall conduction are discussed by examining the impact of the independent parameters on axial pressure distribution (P), interface temperatures ($\theta_{i,l}$ and $\theta_{i,r}$), interface heat fluxes ($q_{i,l}$ and $q_{i,r}$), the average mass flow rate (M), and the average Nusselt number (Nu). Though the calculations were

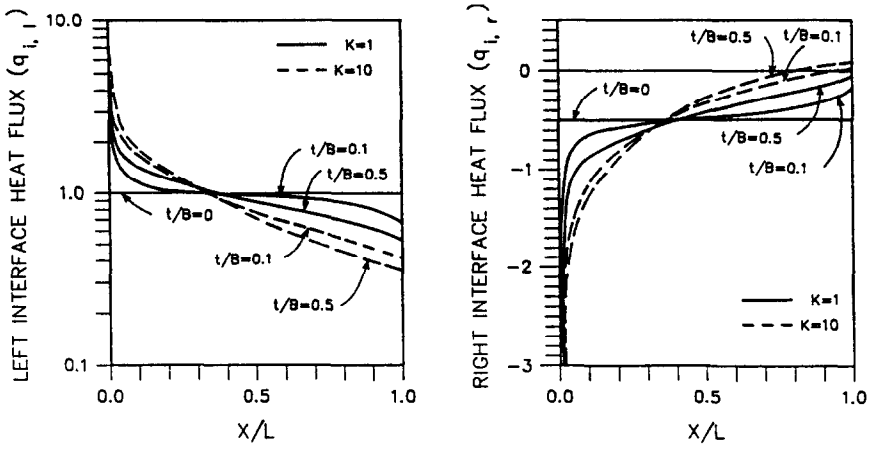

FIG. 3. Axial interface heat flux distribution, $Gr = 100$, $\gamma_H = 0.5$, $L/B = 1$.

performed for a wide range of independent parameters only selected results are detailed.

Interface heat flux

The non-dimensional heat flux at a transverse location is given by

$$q = -\left.\frac{\partial\theta}{\partial Y}\right|_i. \tag{13}$$

Figure 3 shows the axial variation of the left and right interface heat fluxes ($q_{i,l}$ and $q_{i,r}$). The positive values of the left interface heat flux imply that the heat flows from the left wall to the air. Negative values of heat flux for the right interface imply that the heat flows from the right wall to the air. In general, although the external surfaces of the walls are subjected to a uniform heat flux, the heat flux crossing the interfaces is not uniform. From Fig. 3 for $Gr = 10^2$ and $\gamma_H = 0.5$, the interface heat flux in the region closer to the channel entrance is higher than the imposed heat flux on the external surface. This trend reverses in the region closer to the channel exit. Henceforth, the regions closer to the channel entrance and exit are referred to as upstream and downstream regions, respectively. This behavior is more pronounced for higher values of K and t/B. The thermal boundary layer at the channel entrance is thin and has a high heat transfer coefficient, indicating that the ability of the walls to lose heat to the air is higher in the upstream region than in the downstream region. Heat is transported from the downstream to the upstream region within the walls because of wall conduction. Increasing values of K and t/B contribute to an increase in heat transfer within the walls from the downstream to the upstream region.

Figure 4 shows the effect of Gr on the interface heat flux. The case of $\gamma_H = 1$ is considered, where the left and right interface heat fluxes are identical. At lower values of Gr ($= 10$), the interface heat flux is highly nonuniform. A higher Gr ($= 10^4$) represents a shorter channel than for $Gr = 10^2$. In shorter channels, the thermal development is incomplete and the axial gradient of the heat transfer coefficient is less than that for longer channels ($Gr = 10^2$) where the thermal development is complete. This is the reason for the highly non-uniform behavior of the interface heat flux at lower Gr ($= 10$). This non-uniform behavior becomes less pronounced with increase in Gr. The same behavior was observed for $\gamma_H < 1$.

The effect of channel length to channel width ratio (L/B) on interface heat flux is shown in Fig. 5. The interface heat flux ($q_{i,l}$) is more uniform for the case of $L/B = 5$ than for 1 because the conduction heat flux in the wall is inversely proportional to the length, indicating that the wall conduction heat flux is low in the axial direction for higher values of $L/B(= 5)$. Less heat transported in the axial direction within the wall leads to a more uniform interface heat flux.

The axial variation of the right interface heat flux ($q_{i,r}$) for $\gamma_H = 0$ and $Gr = 10^4$ is shown in Fig. 6. Though the external surface is insulated, heat is trans-

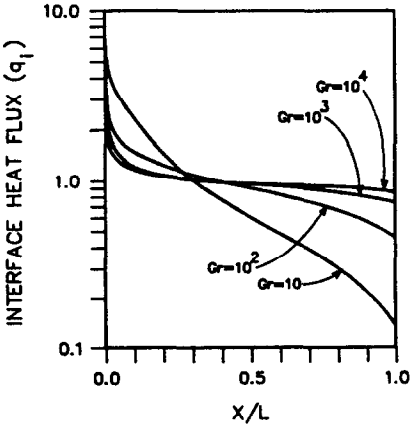

FIG. 4. Axial variations of interface heat flux, $\gamma_H = 1$, $t/B = 0.5$, $K = 1$, $L/B = 1$.

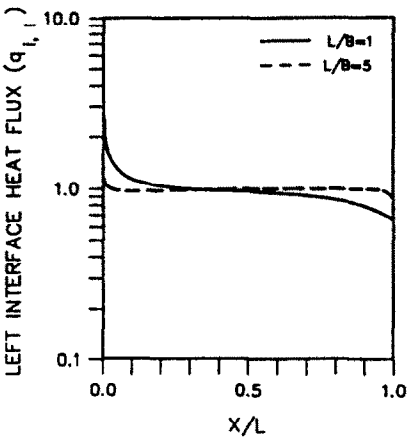

FIG. 5. Effect of L/B on the left interface heat flux, $\gamma_H = 0.5$, $t/B = 0.1$, $K = 1$, $Gr = 10^2$.

ferred from the right wall to the air in the upstream region and from the air to the wall in the downstream region. This is to be expected because heat is transported within the wall from the downstream region to the upstream region.

Interface temperature

The interface temperature distribution for $Gr = 10^4$ and $\gamma_H = 1$ is shown in Fig. 7. The axial gradient of the interface temperature is rather steep when wall conduction effects are absent ($t/B = 0$). The wall conduction effects tend to reduce the interface temperature gradient in the axial direction. Thus the higher the wall conduction effect, the greater the tendency for the interface temperature to flatten out. The same behavior was observed for other values of Gr and γ_H.

The axial variation of the external surface temperature ($\theta_{e,l}$ and $\theta_{e,r}$) for $Gr = 10^4$ and $\gamma_H = 1$ is shown in Fig. 8. As K increases, the difference between the interface and the external surface temperature decreases. This temperature difference increases with t/B because the wall thermal resistance in the Y-direction increases.

Maximum external and interface temperatures

A design engineer needs to know the maximum temperatures that these channels attain. Both the maximum external surface temperature ($\theta_{e,max}$) and the maximum interface temperature ($\theta_{i,max}$) variations with Gr for $\gamma_H = 1$ and 0.5 are shown in Figs. 9 and 10. For the case of $t/B = 0$, the external wall and the interface temperatures are the same. In general, the $\theta_{e,max}$ and $\theta_{i,max}$ decrease with increase in Gr because the heat transfer coefficient increases as Gr increases, leading to lower wall temperatures. The wall conduction effects have less influence on $\theta_{i,max}$ than on $\theta_{e,max}$. Note that the maximum temperature is at the channel exit. Interestingly, as Gr increases, the temperature difference ($\theta_{e,max} - \theta_{i,max}$) increases. At higher Gr ($= 10^4$), the heat transported within the wall in the axial direction is lower (Fig. 4), leading to a higher transverse heat flux at the channel exit within the wall. This results in a higher temperature difference ($\theta_{e,max} - \theta_{i,max}$) and consequently, a higher $\theta_{e,max}$. Similarly, ($\theta_{e,max} - \theta_{i,max}$) decreases with decrease in Gr.

Transverse temperature and velocity distribution

Figure 11 shows the effect of wall conduction on the transverse temperature distribution. Transverse temperature distributions at two axial locations ($X = 0.269$ and 0.886) are chosen for discussion. $X = 0.269$ represents the upstream region, and $X = 0.886$ represents the downstream region. In the upstream region, the temperature is the lowest for the case of no wall conduction ($t/B = 0$). In the upstream region, the temperature increases with wall conduction effects and is a maximum for $t/B = 0.5$ and $K = 10$, attributed to the transport of heat by wall conduction from the downstream to the upstream region. This trend is reversed in the downstream region because the bulk temperature of the air in the absence of wall conduction ($t/B = 0$) is lower as it enters the downstream region and has a greater ability to absorb heat. The same trends were observed for other values of Gr and γ_H.

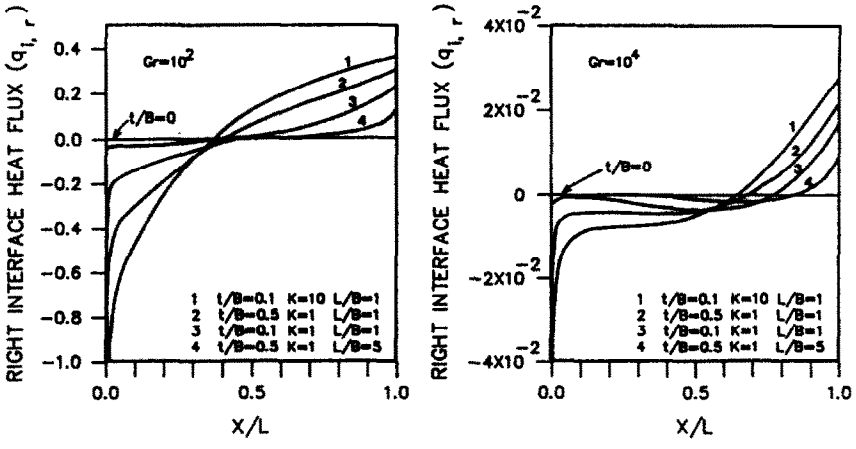

FIG. 6. Axial right interface heat flux distribution, $\gamma_H = 0$.

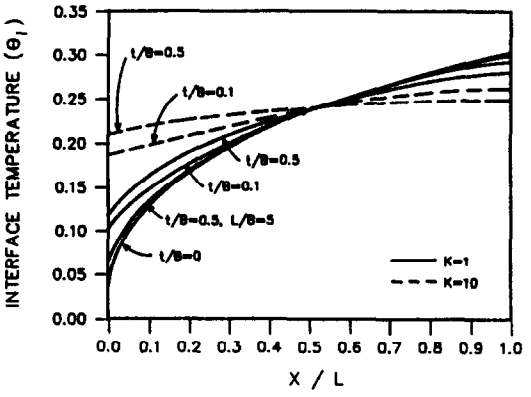

FIG. 7. Axial interface temperature distribution, $Gr = 10^4$, $\gamma_H = 1$, $L/B = 1$.

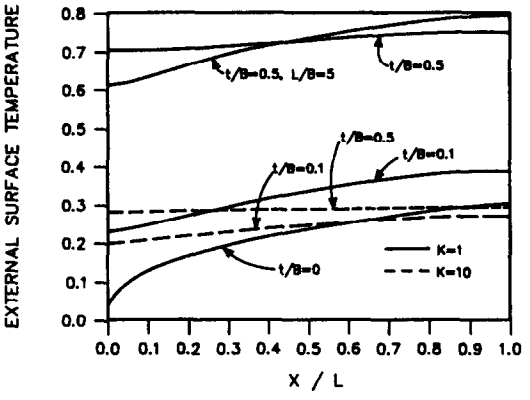

FIG. 8. Axial external surface temperature distribution, $Gr = 10^4$, $\gamma_H = 1$, $L/B = 1$.

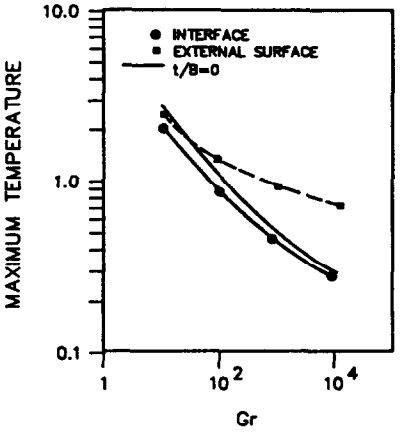

FIG. 9. Variation of maximum temperature with Gr, $\gamma_H = 1$. $t/B = 0.5$, $K = 1$.

The effect of wall conduction on the velocity profiles (U/U_0) is shown in Fig. 12. Wall conduction effects tend to make the interface temperature uniform. Since the velocity (U/U_0) is proportional to the interface temperature, (U/U_0) in the upstream region for $t/b = 0$ is the lowest; this trend is reversed in the

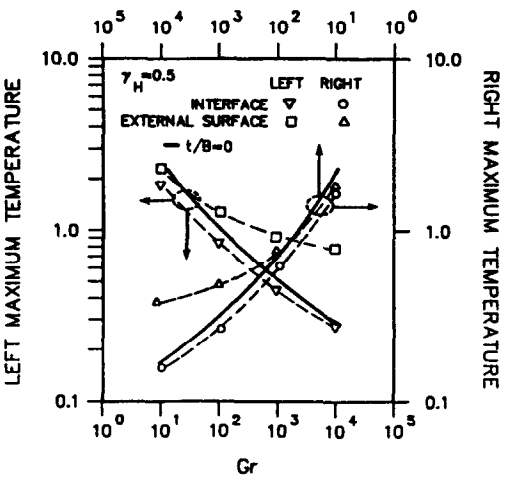

FIG. 10. Variation of maximum temperature with Gr, $\gamma_H = 0.5$, $t/B = 0.5$, $K = 1$.

downstream region. In the downstream region the wall conduction effect influences $(U/U_0)_{max}$ up to a maximum value of 3.5%.

The slope of the velocity profile adjacent to the cold wall in the downstream region (Fig. 12) approaches zero. The point of zero slope is the separation point and downstream of the separation point one can expect flow reversal. However, in our calculations no separation point was observed. It should be recalled that in this analysis the flow is assumed to be of the boundary layer type and flow reversals cannot be predicted. The experimental work of Sparrow *et al.* [8] with water ($Pr \simeq 5$) showed that the recirculation pocket exists near the cold wall in the downstream region under highly asymmetric heating conditions ($\gamma_H = 0$). Recently, Webb and Hill [13] experimentally studied free convective flow of air in an asymmetrically heated channel ($\gamma_H = 0$) at high Rayleigh number (10^7). The experimental results of Webb and Hill [13] compared within 5% of the numerical predictions of ref. [10], which is also based on the boundary layer type flow assumption. Based on these facts it may be concluded that the boundary layer type flow assumption is valid for free convective flow of air ($Pr \simeq 0.7$) in the range of parameters examined in this study. Also, the studies of Sparrow *et al.* [8] for $Pr \simeq 5.0$ have shown that the presence of a recirculation pocket has a negligible effect on the average Nusselt number.

Axial pressure distribution

The effect of wall conduction on the pressure distribution is shown in Fig. 13 for $Gr = 10^2$ and $\gamma_H = 0.5$. P_{min} is lowest for the case where the wall conduction is absent $(t/B = 0)$. In general, P_{min} increases with increase in t/B and K. This same behavior was observed for other values of Gr and γ_H. Figure 14 shows the variation of P_{min} with Gr. As Gr increases, both P_{min} and wall conduction effects decrease.

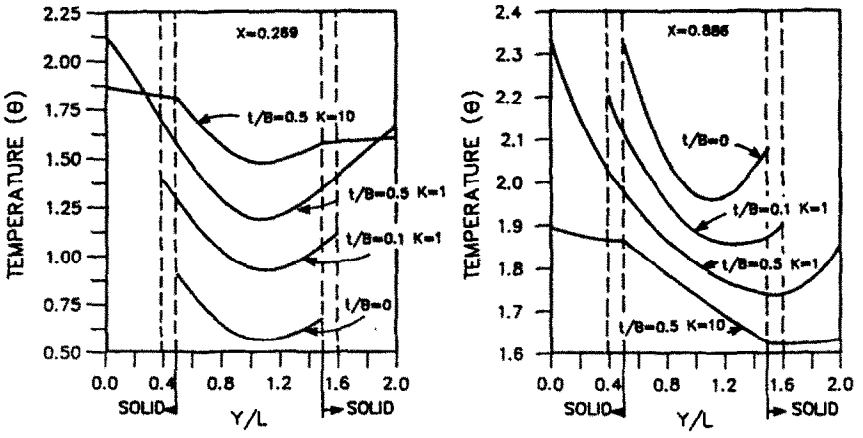

FIG. 11. Transverse temperature distribution, $Gr = 10$, $\gamma_H = 0.5$, $L/B = 1$.

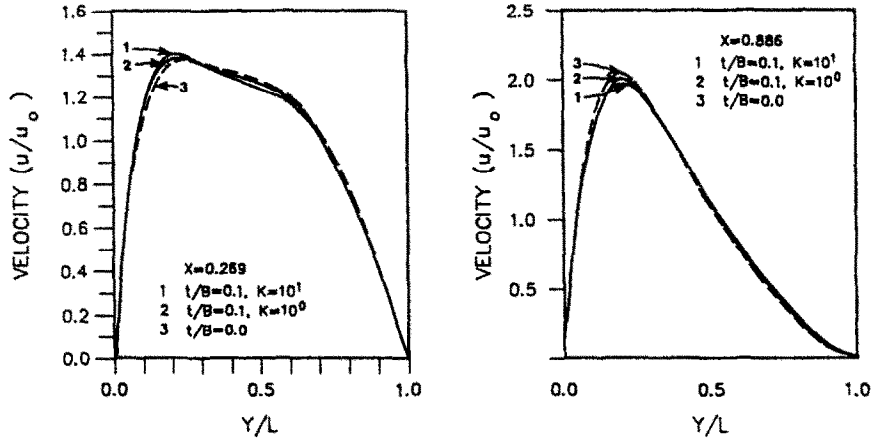

FIG. 12. Transverse velocity distribution, $Gr = 10^4$, $\gamma_H = 0$, $L/B = 1$.

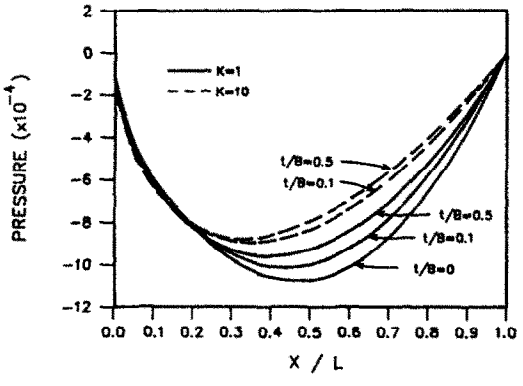

FIG. 13. Axial pressure distribution, $Gr = 10^2$, $\gamma_H = 0.5$, $L/B = 1$.

Mass flow rate

The non-dimensional mass flow rate of air (M) is defined by

$$M = \frac{u_0 B^2}{\nu L\, Gr} = \int_{Y_{1,1}}^{Y_{1,2}} U \, dY. \tag{14}$$

Figure 15 shows the impact on mass flow rate (M) for different asymmetric heating parameters and $L/B = 1$ and 5. The mass flow rate increases with increase in Gr as expected since the buoyancy forces are higher at higher values of Gr. The influence of wall conduction on M decreases with increase in Gr but increases with decrease in γ_H. For $\gamma_H = 1$, the wall conduction effects increase the mass flow rate by as much as 30% for $Gr = 10$. For the same value of γ_H, the wall conduction effects increase the mass flow rate by as much as 8% at $Gr = 10^4$. These calculated percentage increases are higher bounds for symmetric heating conditions ($\gamma_H = 1$). For $\gamma_H < 1$, however, these percentages increase further and are the lower bounds. The increase of mass flow rate with wall conduction effects is attributed to an increase in the average interface temperatures. The increase in average interface temperature is lower for $Gr = 10^4$ than for 10. It is clear from Fig. 15 that when L/B is increased from 1 to 5 the change in mass flow rate is negligible because L/B has a minimum impact on interface heat flux and temperatures (Figs. 5 and 7).

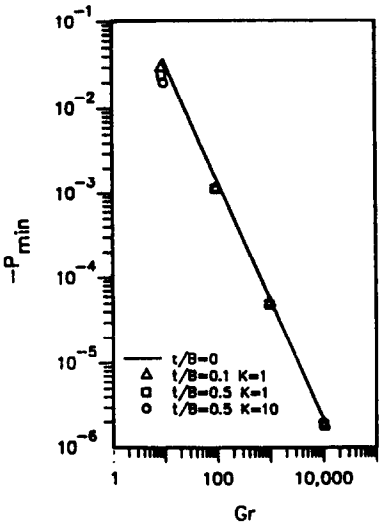

FIG. 14. Effect of wall conduction on minimum pressure, $\gamma_H = 1$, $L/B = 1$.

Local Nusselt numbers

The local Nusselt numbers for the left and right interfaces are defined as

$$Nu_{i,l} = \frac{q_{i,l}}{\theta_{i,l}} \tag{15}$$

$$Nu_{i,r} = \frac{q_{i,r}}{\theta_{i,r}}. \tag{16}$$

The axial variation of the local Nusselt number at the left and right interfaces for $\gamma_H = 0.5$ is shown in Fig. 16. As expected, the local heat transfer coefficient is higher for higher values of Gr ($=10^4$). The gradient of the heat transfer coefficient for $Gr = 10^4$ is less steep than for $Gr = 10$ because $Gr = 10^4$ represents a shorter channel and thermal development is incomplete.

Average Nusselt number

The variation of average Nusselt number defined by equation (10) with the average Grashof number ($\overline{Gr}$) is shown in Fig. 17. The average Grashof number ($\overline{Gr}$) is defined by

$$\overline{Gr} = Gr\frac{(1+\gamma_H)}{2}. \tag{17}$$

Here $\overline{Nu}$ represents an overall heat transfer coefficient of a channel subjected to asymmetric heating. The solid line indicates the case where the wall conduction is absent ($t/B = 0$). The wall conduction effects decrease $\overline{Nu}$; this trend is more pronounced at lower values of $\overline{Gr}$. Note that this observation is consistent with that made earlier that the mass flow rate increases with increase in wall conduction effects. In general, the wall conduction effects increase the average interface temperatures, leading to higher buoyancy forces, and consequently, higher mass flow rates. Nevertheless, $\overline{Nu}$ decreases with increase in average interface temperature because they are inversely proportional (equation (10)). For $\overline{Gr} = 5$, the decrease in $\overline{Nu}$ is as low as 22%: at $\overline{Gr} = 10^4$, the decrease is 6%. The increase in L/B from 1 to 5 has little impact on $\overline{Nu}$.

CONCLUSIONS

In this investigation of the effect of wall conduction on laminar free convection between vertical plates the external surfaces of which are subjected to asymmetric

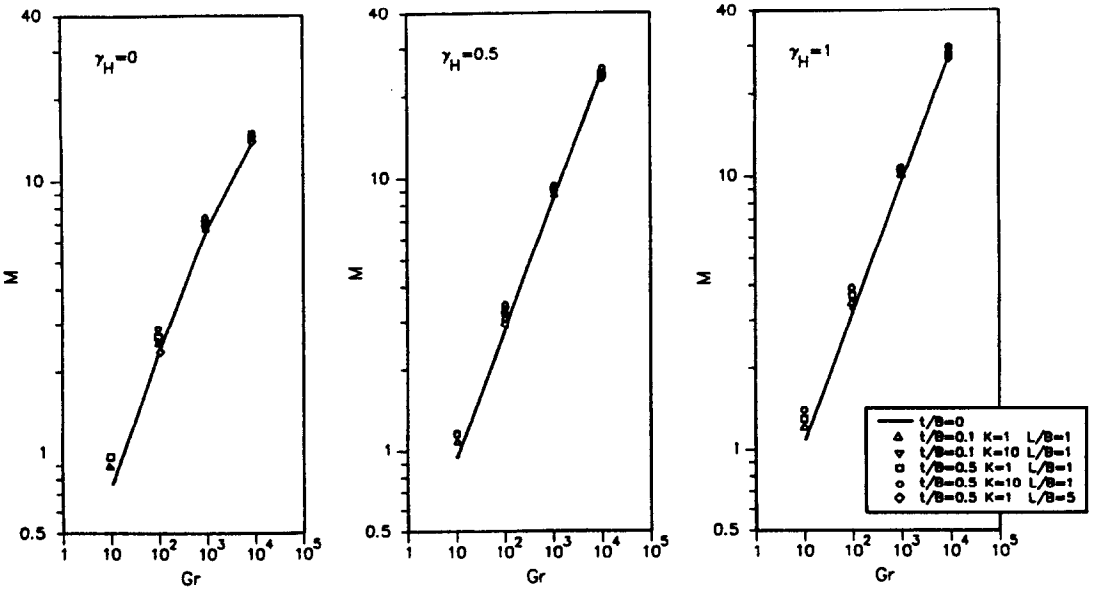

FIG. 15. Effect of wall conduction on mass flow rate.

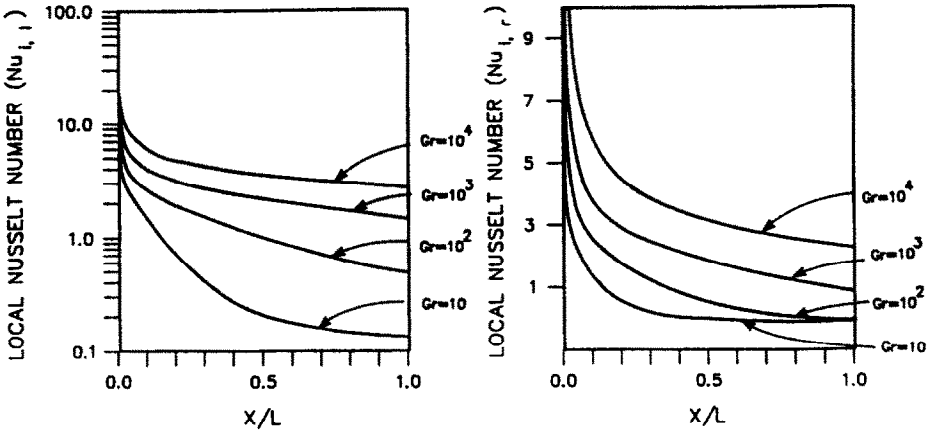

FIG. 16. Variation of local Nusselt number with Gr, $\gamma_H = 0.5$, $t/B = 0.5$, $K = 10$, $L/B = 1$.

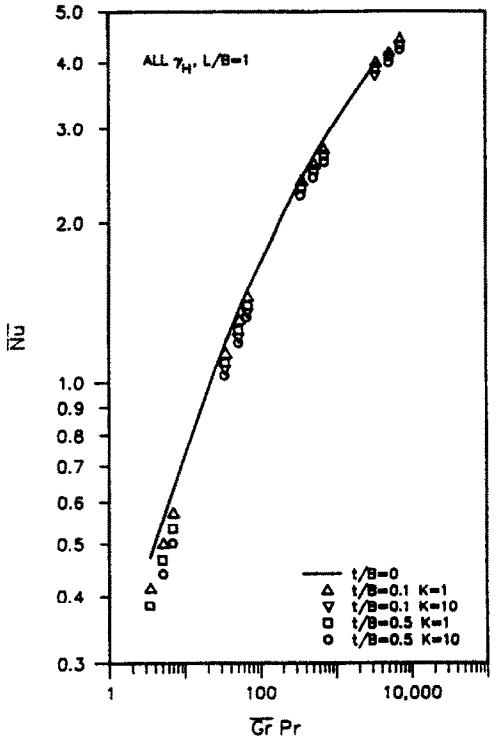

FIG. 17. Effect of wall conduction on average Nusselt number.

heat fluxes, the governing equations are solved by an implicit finite difference scheme. Calculations were made for a wide range of independent parameters (Gr, t/B, K, L/B, and γ_H). The mass flow rate of air increases with increase in buoyancy forces. Increase in t/B and K results in higher interface temperatures, leading to higher buoyancy forces. The key conclusions are given as follows.

(1) The interface heat fluxes ($q_{i,l}$ and $q_{i,r}$) are extremely nonuniform (in the X-direction) even though the external surfaces of the walls are subjected to uniform heat flux. The nonuniformity in the interface heat flux distribution increases with wall conduction effects (t/B and K) and also increases with decrease in Gr and L/B.

(2) The increase in t/B and K tends to make both interface and external surface temperature distributions uniform in the axial direction. The impact of wall conduction on interface temperature decreases with increase in Gr.

(3) The maximum influence of wall conduction on U/U_0 is 3.5%.

(4) Wall conduction has a significant impact on mass flow rate. Mass flow rate (M) increases with increase in t B and K. For symmetric heating ($\gamma_H = 1$), the mass flow rate increases by 30% for $Gr = 10$ and by 8% for $Gr = 10^4$.

(5) The increase in mass flow rate is greater for asymmetric heating.

(6) The wall conduction effect decreases the average Nusselt number ($\overline{Nu}$). For $\overline{Gr} = 5$, the reduction in $\overline{Nu}$ is 22%; for $\overline{Gr} = 10^4$, the reduction is 6%.

Acknowledgement—This research was supported in part by Texas A&M Engineering Excellence Funds. Computing facilities were made available by the College of Engineering and Texas A&M University Computing Services.

REFERENCES

1. W. Elenbass, Heat dissipation of parallel plates by free convection, *Physica* **9**, 1–28 (1942).
2. E. M. Sparrow and P. A. Bahrami, Experiments on natural convection from vertical parallel plates with either open or closed edges, *ASME J. Heat Transfer* **102**, 221–227 (1980).
3. R. A. Wirtz and R. J. Stutzman, Experiments on free convection between vertical plates with symmetric heating, *ASME J. Heat Transfer* **104**, 501–507 (1982).
4. L. F. Azevedo and E. M. Sparrow, Natural convection in open-ended inclined channels, *ASME J. Heat Transfer* **107**, 893–901 (1985).
5. J. R. Bodoia and J. F. Osterle, The development of free convection between heated vertical plates, *ASME J. Heat Transfer* **84**, 40–44 (1962).
6. W. Aung and G. Worku, Developing flow and flow reversal in a vertical channel with asymmetric wall temperatures, *ASME J. Heat Transfer* **108**, 299–304 (1986).

7. W. Aung and G. Worku, Theory of fully developed, combined convection including flow reversal, *ASME J. Heat Transfer* **108**, 485–488 (1986).
8. E. M. Sparrow, G. M. Chrysler and L. F. Azevedo, Observed flow reversals and measured-predicted Nusselt numbers for natural convection in a one-sided heated vertical channel, *ASME J. Heat Transfer* **106**, 325–332 (1984).
9. W. Aung, Fully developed laminar free convection between vertical plates heated asymmetrically, *Int. J. Heat Mass Transfer* **15**, 1577–1580 (1972).
10. W. Aung, L. S. Fletcher and V. Sernas, Developing laminar free convection between flat plates with asymmetric heating, *Int. J. Heat Mass Transfer* **15**, 2293–2308 (1972).
11. J. R. Carpenter, D. G. Brigs and V. Sernas, Combined radiation and developing laminar free convection between vertical flat plates with asymmetric heating, *ASME J. Heat Transfer* **98**, 95–100 (1976).
12. T. Burch, T. Rhodes and S. Acharya, Laminar natural convection between finitely conducting vertical plates, *Int. J. Heat Mass Transfer* **28**, 1173–1186 (1985).
13. B. Webb and D. P. Hill, High Rayleigh number laminar natural convection in an asymmetrically heated vertical channel, *ASME J. Heat Transfer* **111**, 649–656 (1989).

EFFET DE LA CONDUCTION PARIETALE SUR LA CONVECTION NATURELLE ENTRE DES PLAQUES VERTICALES DIFFEREMMENT CHAUDES: DENSITE DE FLUX THERMIQUE UNIFORME A LA PAROI

Résumé—Dans l'étude de l'effet de la conduction pariétale sur la convection naturelle laminaire entre des plaques verticales différemment chauffées, on utilise un schéma implicite aux différences finies pour résoudre les équations. Les paramètres indépendants sont identifiés comme étant le nombre de Prandtl (*Pr*), le nombre de Grashof (*Gr*), le rapport des conductivités du solide et de l'air (*K*), le rapport de l'épaisseur de la paroi à la largeur du canal (t/B), le rapport de la hauteur du canal à la largeur (L/B) et le paramètre d'asymétrie du chauffage (γ_H). On discute l'effet de la conduction sur l'écoulement naturel d'air dans les conditions de chauffage disymétrique ($\gamma_H = 1{,}0$; 0,5 et 0). Des calculs sont faits pour $K = 1$ et 10, $t/B = 0{,}1$ et 0,5, $Gr = 10$–10^4, $L/B = 1$ et 5. L'accroissement maximal de débit masse d'air est de 30% pour un chauffage symétrique, du fait de la conduction pariétale. La diminution la plus grande du nombre de Nusselt du fait de la conduction pariétale est de 22%. Les effets de cette conduction sont pour les faibles *Gr* plus significatifs que pour les *Gr* élevés.

EINFLUSS DER WÄRMELEITUNG IN DER WAND AUF DIE FREIE KONVEKTION ZWISCHEN ASYMMETRISCH BEHEIZTEN, SENKRECHTEN PLATTEN BEI AUFGEPRÄGTER WÄRMESTROMDICHTE

Zusammenfassung—In dieser Arbeit wird der Einfluß der Wärmeleitung in der Wand auf die laminare freie Konvektion zwischen asymmetrisch beheizten, senkrechten Platten untersucht. Die Grundgleichungen werden mit einem impliziten Finite-Differenzen-Verfahren gelöst. Die maßgeblichen Einflußgrößen sind die Prandtl-Zahl (*Pr*), Grashof-Zahl (*Gr*), das Verhältnis der Wärmeleitfähigkeiten von Feststoff und Luft (*K*), das Verhältnis von Wanddicke zu Plattenabstand (t/B), das Verhältnis von Kanalhöhe zu Plattenabstand (L/B) und der Parameter für die asymmetrische Beheizung (γ_H). Der Einfluß der Wärmeleitung in der Wand auf die freie Konvektionsströmung von Luft unter den Bedingungen einer asymmetrischen Beheizung ($\gamma_H = 1{,}0$; 0,5; und 0) wird diskutiert. Die Berechnungen werden ausgeführt für $K = 1$ und 10, für $t/B = 0{,}1$ und 0,5, für $Gr = 10$ bis 10^4 und für $L/B = 1$ und 5. Die maximale Erhöhung des Luftmassenstroms beträgt bei symmetrischer Beheizung infolge der Wärmeleitung in der Wand 30%. Die maximale Verkleinerung der mittleren Nusselt-Zahl infolge der Wärmeleitung in der Wand beträgt 22%. Der Einfluß der Wärmeleitung in der Wand nimmt mit steigender *Gr*-Zahl ab.

ВЛИЯНИЕ ТЕПЛОПРОВОДНОСТИ СТЕНКИ НА СВОБОДНУЮ КОНВЕКЦИЮ МЕЖДУ АСИММЕТРИЧНО НАГРЕТЫМИ ВЕРТИКАЛЬНЫМИ ПЛАСТИНАМИ: СЛУЧАЙ ОДНОРОДНОГО ТЕПЛОВОГО ПОТОКА НА СТЕНКЕ

Аннотация—С использованием неявной конечно-разностной схемы исследуется влияние теплопроводности стенки на свободную конвекцию при ламинарном течении. Найдено, что определяющими независимыми параметрами являются число Прандтля *Pr*, число Грасгофа *Gr*, соотношение коэффициентов теплопроводности твердого тела и воздуха *K*, отношение толщины стенки к ширине канала t/B, отношение высоты канала к его ширине L/B и параметр асимметричного нагрева γ_H. Обсуждается влияние теплопроводности стенки на свободноконвективное течение воздуха в условиях асимметричного нагрева ($\gamma_H = 1{,}0$; 0,5 и 0). Выполнены расчеты для $K = 1$ и 10, $t/B = 0{,}1$ и 0,5; $Gr = 10$–10^4, а также $L/B = 1$ и 5. Максимальное увеличение массового расхода воздуха при симметричном нагреве за счет теплопроводности стенки составляет 30%. Максимальное уменьшение среднего значения числа Нуссельта, обусловленное теплопроводностью стенки, равно 22%. В случае течения при низких значениях *Gr* эффект теплопроводности стенки более значителен, чем при высоких значениях *Gr*.